buildings

MDPI

Article

Experimental Study on Mechanical Properties of Reinforced Soil and Frame Beam Anchor Combination System

Jiangfei He [1,2,*] and Leihua Yao [3]

[1] School of Civil and Architectural Engineering, Liaoning University of Technology, Jinzhou 121001, China
[2] Shaanxi Institute of Engineering Prospecting, Xi'an 710068, China
[3] School of Engineering and Technology, China University of Geosciences (Beijing), Beijing 100083, China; yaolh@cugb.edu.cn
* Correspondence: tjhejf@lnut.edu.cn

Abstract: To address issues with excessive displacement, deformation, and insufficient load bearing capacity in high-fill-reinforced soil-retaining walls, a novel reinforced soil–frame anchor combination system was developed. Despite the limited existing research on its mechanical properties and synergy, a physical model test was conducted to investigate the system's behavior. The test focused on the horizontal displacement of the frame beam wall, grid strain, wall back earth pressure, and anchor strain. Results indicated that anchor prestress effectively controlled horizontal deformation, limiting it to 65% of the original displacement value. Additionally, as the top load increased, strain in the bottom bars showed minor changes, while strain in the middle and upper bars exhibited significant sensitivity to load variations. The application of anchor prestress reduced strain in each reinforcement layer, enhancing the geogrid's load bearing capacity. Furthermore, anchor prestress altered the distribution of earth pressure within the system, establishing a synergistic relationship between reinforced soil and frame beam anchors. This stress transfer mechanism improved overall system performance, as demonstrated in the test. Overall, the study confirmed the benefits and superior performance of the combined system.

Keywords: reinforced soil; anchor; frame beam; synergistic action; mechanical properties

check for updates

Citation: He, J.; Yao, L. Experimental Study on Mechanical Properties of Reinforced Soil and Frame Beam Anchor Combination System. *Buildings* **2024**, *14*, 1372. https://doi.org/10.3390/buildings14051372

Academic Editor: Flavio Stochino

Received: 24 March 2024
Revised: 30 April 2024
Accepted: 7 May 2024
Published: 10 May 2024

1. Introduction

Due to unreasonable excavation, high and steep slopes often lose stability during development and construction in mountainous areas. In order to quickly repair high-slope disasters, using a single retaining structure or conventional composite structure cannot meet the needs of engineering construction. In order to address the problems of steep slopes and large lateral deformation displacement in high-fill projects under the constraints of limited construction space for backfilling and urgent repair schedules, a "reinforced soil composite retaining structure" is proposed. This involves using a narrow reinforced soil-retaining wall filled in front of the slope collapse zone, similar to the shored mechanically stabilized earth wall (SMSEWall) in the American code [1], also commonly referred to as "narrow geosynthetic reinforced Soil wall". Some preliminary studies have been conducted on short reinforced soil-retaining walls. Yang et al. [2–4] believe that there is tensile stress on the contact surface between the short reinforced soil and its subsequent wall, and due to insufficient lengths of reinforcement, cracks are easily generated at the contact boundary. Lee et al. [5] showed that there is a possibility of fracture of the reinforcement within the short-reinforced condition under the effect of overloading on the slope top. Xu Chao et al. [6–8] conducted experimental research on the soil pressure law of short reinforced soil-retaining walls and explored the failure modes of short reinforced soil-retaining walls.

In terms of traditional slope anchoring technology, Zhou Yong and Zhu Yanpeng [9–11] have conducted theoretical, design method, and engineering application research on frame beam anchors. Fu Xiao [12] established a shaking table test to study the dynamic response law of frame anchor cables and frame anchor cable–anti-slide pile-reinforcing slopes, revealing the collaborative mechanism and mechanical response law of frame anchor cables–anti-slide piles during earthquakes, and proposing seismic design methods. Based on the assumption that the simplified inertial effect of the anchor rod is equivalent to the external equivalent mass at the end of the anchor rod, Dong Jianhua [13] derived the dynamic equation of the collaborative effect of frame anchors, obtained the axial law of the anchor rod under earthquakes, and compared it with numerical calculations and shaking table tests to verify the rationality of the calculation model. He Siming [14] used the upper limit method of limit analysis combined with Hoek–Brown failure criteria to establish a formula for the pre-reinforcement load of rock slope and analyzed and calculated the permanent displacement value under earthquake action. Luo Jiwei [15] proposed a prestressed anchor–cable collaborative support system, studied the mechanical behavior of the prestressed anchor–cable collaborative support system through field monitoring, analyzed the mechanism of prestressed anchor–cable collaborative support, and achieved effective support for ultra-large-span tunnels. Long Jingkui [16] applied the principle of collaborative action to a coal mine roadway surrounding rock control, constructed an evaluation method for a collaborative anchoring system, established a mechanism for the collaborative anchoring of anchor rods and anchor cables, and obtained a realization method for a collaborative action mechanism. Du Yunxing [17] used a similar ratio model test to study a reinforced soil and prestressed anchor combination structure retaining wall. Compared with ordinary reinforced soil-retaining walls, the displacement of this hybrid reinforced soil panel and the settlement of the wall top were significantly reduced.

The current reinforced soil composite structures mainly include micro pile-reinforced soil-retaining walls [18,19], balance weight retaining wall-reinforced soil-retaining walls [20], buttress-retaining wall-reinforced soil-retaining walls [21], and anti-slip pile-reinforced soil-retaining walls [22,23]. However, the above combination forms cannot achieve ideal results in the rapid repair of high and steep slopes. In order to break through the technical bottleneck of existing support structures and solve the problems of excessive displacement deformation and insufficient bearing capacity in the treatment and reinforcement of high slopes, this paper proposes a reinforced soil–frame anchor combination system [24,25] based on a thorough examination of traditional anchoring slope technology, and successfully applies it to a certain high- and steep-slope project. At present, there is limited research on the composite structure of reinforced soil frame beam anchors, and the collaborative mechanism between frame beam anchors and reinforced soil is not yet clear. Its mechanical properties and engineering applicability also need to be verified. Therefore, this paper designs a scaled test model of reinforced soil–frame beam anchors, revealing the collaborative process of reinforced soil and frame beam anchors and the mechanical performance characteristics of the composite system, in order to provide theoretical guidance and technical support for its design and application in landslide control.

2. Test Scheme

2.1. Test Model

2.1.1. Model Box

This study focuses on the simulation model of the supporting structure of Mingdi No. 1 slope in Tongchuan, Shaanxi Province, China. The retaining wall in the model had dimensions of 30 m in length and 20 m in height, a two-level slope, and a slope ratio of 1:0.2. Due to site constraints and limitations in test equipment, a scale ratio of 1:10 was chosen for the model test [26,27]. The retaining wall in the model test had dimensions of 3.0 m in length and 2.0 m height, and a slope ratio of 1:0.2 (Figures 1 and 2). This study focuses on analyzing the mechanical properties of reinforced soil and frame beam anchors. The test model box utilized measured 3.2 m $\times$ 1.0 m $\times$ 2.2 m (length $\times$ width $\times$ height). Prior to the layering construction process of filling soil, a layer of plastic film was applied to the inner wall of the test box to minimize the friction effect on the system. Due to the limitations of the physical model size, it was challenging to guarantee that the material selection, loading path settings, construction process restoration, and other simulations aligned perfectly with full-scale testing. As a result, future research will include field tests of the combined system and in-depth studies on the synergistic effects of the combined system to address the current research limitations.

Figure 1. Picture of model test box.

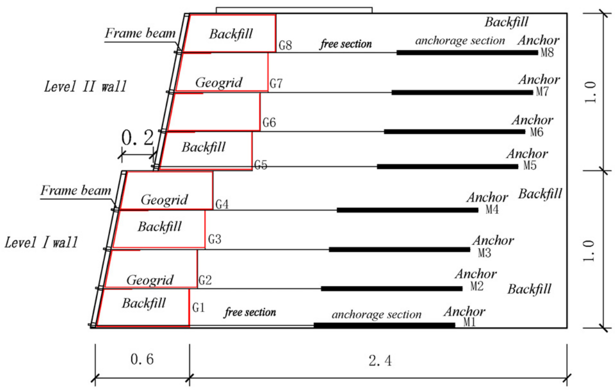

Figure 2. Schematic view of model box (unit: m).

2.1.2. Data Measurement and Collection Equipment

The test requires earth pressure cells, resistance strain gauges, dial indicators, and anchor dynamometers for measurement, while the collection equipment required includes resistance strain gauges, and dynamic and static resistance strain gauges. The specific parameters of the test components can be found in Table 1. The location of the test components is shown in Figures 3–6.

Table 1. Specific parameters of the test components.

Name	Model	Measuring Range	Quantity
Earth pressure cells	DMTY-402	0.3 Mpa	7
Resistance strain gauges	BFH120-1AA-S	120 ± 2 (Ω)	64
Dial indicators	0~50 mm	50 mm	8
Smart reader	XB-6000	1	1
Anchor dynamometers	DMHZ	1 T	8
Resistance strain gauges	DH3816	12	1
Dynamic and static resistance strain gauges	DM-YB1820	9	1

Figure 3. Earth pressure cells of model test.

Figure 4. Resistance strain gauges of model test.

Figure 5. Dial indicator of model test.

Figure 6. Anchor dynamometers of model test.

The earth pressure box was positioned behind the frame beam and between the reinforced soil and the original slope, as illustrated in Figure 3. Prior to each layer of backfill soil being placed, the earth pressure box was positioned in a predetermined location. Strain gauges were primarily mounted on geogrids and anchors, as depicted in Figure 4. These strain gauges were installed in advance during the preparation of geogrids and anchors. The dial indicator was situated in front of the frame beam, as shown in Figure 5. This dial indicator was mounted after the model was constructed but before testing commenced. The anchor dynamometer was positioned at the end of the anchor, as illustrated in Figure 6. This anchor dynamometer was installed promptly after each layer of anchors was placed and before backfilling with reinforced soil.

2.2. Experimental Materials

2.2.1. Soil Layer Material

During the experiment, undisturbed samples of loess soil were used after removing particles larger than 5 mm. The filling mixture consisted of original soil and fine sand in a ratio of 0.728:0.272, with a density of 16.8 kN/m^3. The moisture content of the test soil was kept at around 15% to match the slope material. When filling soil materials, the loess was initially compacted and backfilled in incremental steps within the model box, achieving a controlled compaction degree of 95% to replicate the original slope area. The reinforced soil area was then filled according to the design, layer by layer at a depth of 20 cm, and compacted uniformly. The compaction degree of the fill can be assessed using the ring knife method, while the moisture content of the fill can be checked using the drying method. After the experiment, the internal friction angle of the reinforced soil layer was measured at 26.7°, cohesive force was measured at 5.6 kPa, Poisson's ratio was measured at 0.35, and the elastic modulus was measured at 7.8 MPa.

2.2.2. Reinforcement Material

The backfill soil layer was filled in layers according to the established compaction degree, with a filling thickness of 20 cm for each layer. The geogrid was laid on the soil layer, as shown in Figure 7. The soil layer was filled in sequence, and the geogrid was laid until the design wall height was reached. Adopting the bidirectional geogrid (Figure 7), its main characteristics and specifications are shown in Table 2.

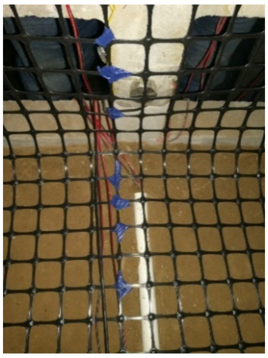

Figure 7. Geogrid used in tests.

Table 2. Characteristics of geogrid.

Thickness/mm	Mesh/(cm × cm)	Tensile Strength/(kN·m^{-1})	2% Strain Strength/(kN·m^{-1})	5% Strain Strength/(kN·m^{-1})
0.76	4 × 4	12.4	4.1	8.5

2.2.3. Anchor

The anchor material was comprised of plain steel bars with a diameter of 8.0 mm (Figure 8). The anchorage section was pre-fabricated with cement mortar, while the free section was threaded through PVC pipes. Each layer of the anchor had a total length of

2.2 m, with the anchorage section measuring 0.8 m. The diameter of the anchor body was 120 mm. The anchor head was secured in place with nuts.

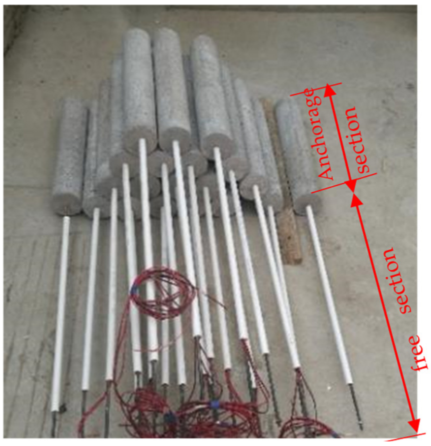

Figure 8. Anchor used in tests.

2.2.4. Frame Beam

The frame beam was made of concrete and had a cross-section measuring 40 mm × 40 mm (Figure 9). The primary reinforcement was 6 mm diameter aluminum wire, with a hoop reinforcement made of 2.4 mm diameter iron wire spaced at 200 mm intervals (Figure 10).

Figure 9. Frame beam used in tests.

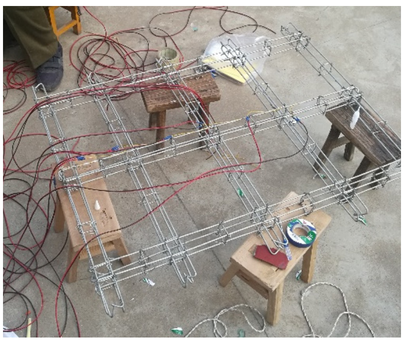

Figure 10. Frame beam rebar used in tests.

2.3. Test Loading Scheme

The primary objective of this study was to investigate the coordinated deformation and mechanical properties of frame beam anchors and reinforced soil. The internal backfilling of the model was completed prior to the external reinforced soil backfilling. The testing process consisted of two steps, with each level being backfilled four times. After the model was filled, it was left to settle for a period of 10 days (240 h) before loading commenced. Prior to loading, a prestress of 1.0 kN was applied to anchor the system. Subsequently, the load was incrementally increased on the top part of the model in four stages (5 kPa–10 kPa–15 kPa–20 kPa). Finally, a prestress of 3.0 kN was applied to the entire anchor. The model test involved monitoring the horizontal displacement of the retaining wall, the strain of the reinforcement, and the earth pressure. The experimental setup is illustrated in Figure 11. During the testing process, we conducted multiple observations on each set of data, performed comparative verification and analysis of the data, and removed any abnormal data to ensure the reliability of the test result data.

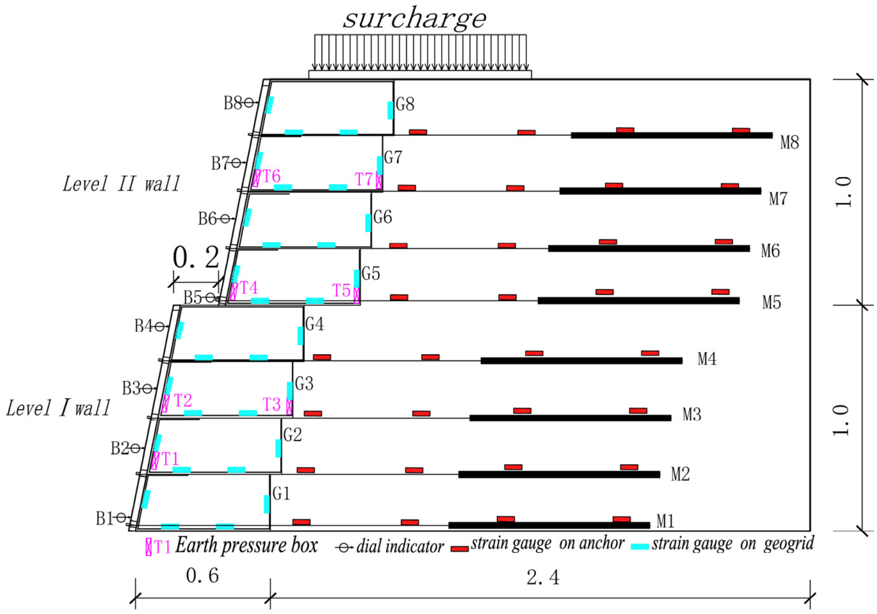

Figure 11. Arrangement of monitoring instruments (unit: m).

3. Testing Results and Analysis

3.1. Horizontal Displacement

Figure 12 displays the horizontal deformation curve of the wall. The term 'before loading' in the figure refers to the monitoring value obtained after the model was filled and left standing for 10 days (240 h). As shown in Figure 8, significant deformation occurs on the wall surface after the completion of the four loadings. The maximum horizontal displacement of the test model is 1.8 mm, corresponding to a maximum horizontal deformation of 18 mm on the prototype. This deformation fulfills the requirements of anchor and geogrid in the combined system. It is characterized through strain, demonstrating the feasibility of this design model test. The horizontal deformation resulting from primary and secondary loading is particularly pronounced, mainly due to soil compaction. Therefore, the compaction of the backfill material plays a crucial role in the system's performance. It is advised to strictly regulate compaction during construction.

Figure 12 illustrates that the horizontal deformation value of the Level II wall was notably higher compared with that of the Level I wall. Following four loadings, the Level I wall's maximum horizontal deformation displacement was merely 62% of that of the Level II wall. This difference can be attributed to two main factors. Firstly, the stress reduction effect was due to the presence of steps between the Level I wall and the Level II wall. Secondly, the large stress diffusion angle in the reinforced soil area resulted in the additional stress from the load on the model's top, having a minimal impact on the frame beam.

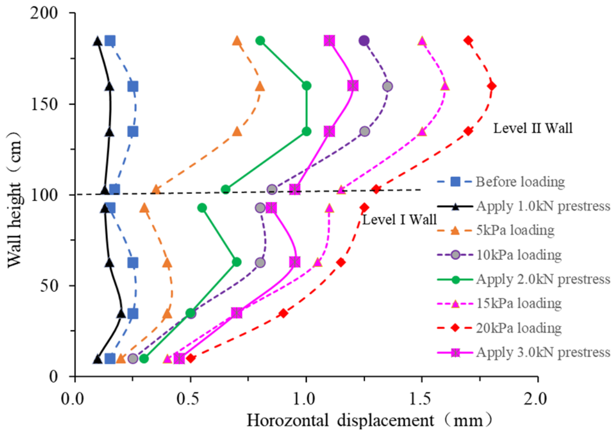

Figure 12. Horizontal deformation distribution curves along wall height.

The horizontal deformation curves of Level I and II walls in Figure 12 are both shaped like ')', with the peak value located approximately one-third of H (where H represents the wall height) from the top of each wall Level. The figure demonstrates that applying anchor prestress twice can reduce the horizontal displacement of the wall. The second application of prestress results in the horizontal displacement deformation of the wall reaching 65% of the original displacement deformation value. Upon analysis, it is observed that the combined system, when subjected to top load, collectively supports the external load through stress transfer. The presence of anchor prestress ensures coordinated deformation between the frame beam anchor and reinforced soil, leading to a beneficial synergistic effect. Anchor prestress plays a crucial role in controlling the displacement deformation of the wall.

3.2. Geogrid Strain

Figure 13 illustrates the geogrid strain distribution curve at different load levels. The analysis of this curve reveals a non-linear distribution of strain across each layer of grid bars as the load increases. A notable pattern observed is that the strain on each bar is minimal on the wall side, with a smaller increase as the load grows. This phenomenon can be attributed to the weakening of strain deformation on the face-side geogrid due to the synergistic effect of the frame beam anchor.

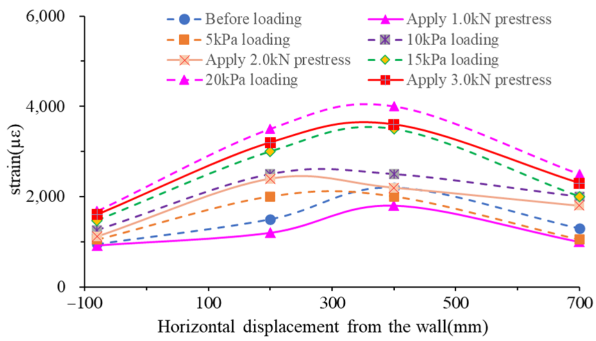

(**a**) First layer of geogrid (Level I wall)

Figure 13. *Cont.*

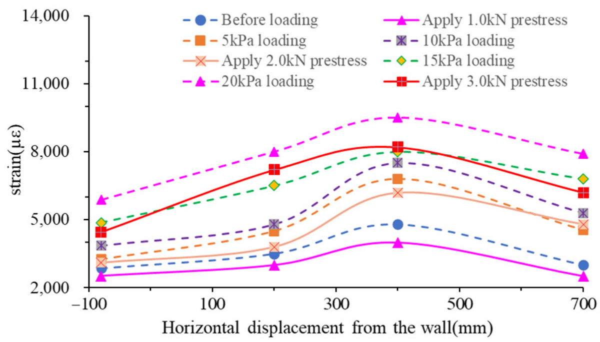

(**b**) Second layer of geogrid (Level I wall)

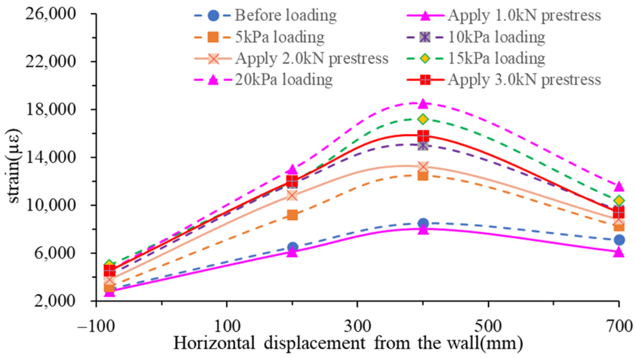

(**c**) The third layer of geogrid (Level I wall)

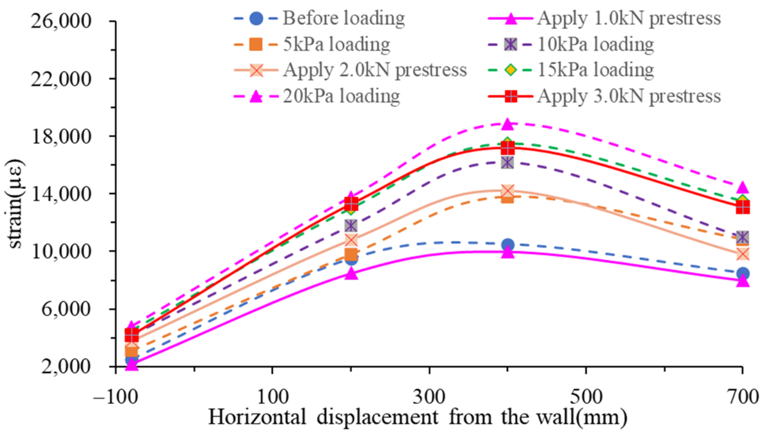

(**d**) Fourth layer of geogrid (Level I wall)

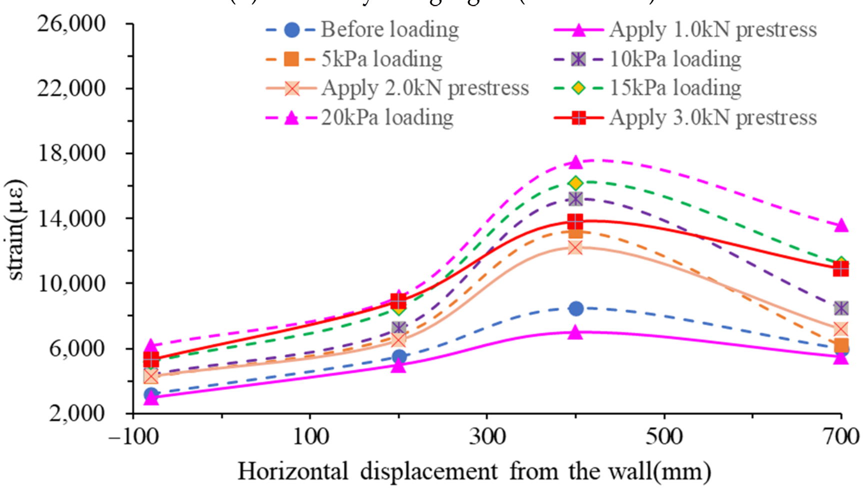

(**e**) Fifth layer of geogrid (Level II wall)

Figure 13. *Cont.*

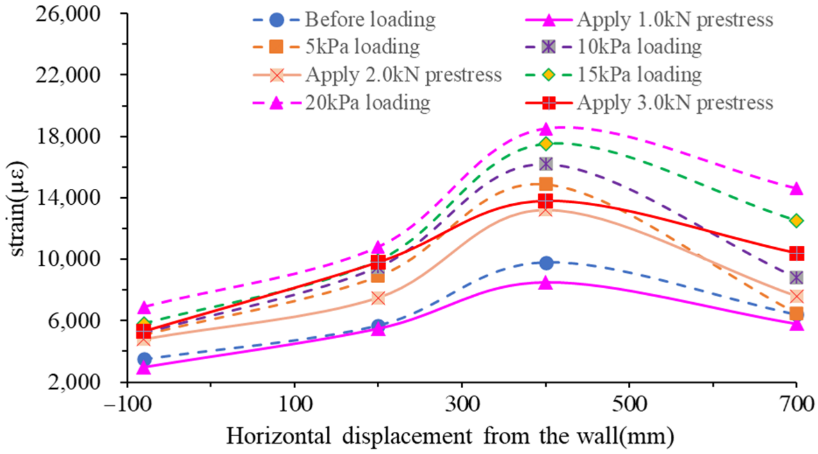

(**f**) Sixth layer of geogrid (Level II wall)

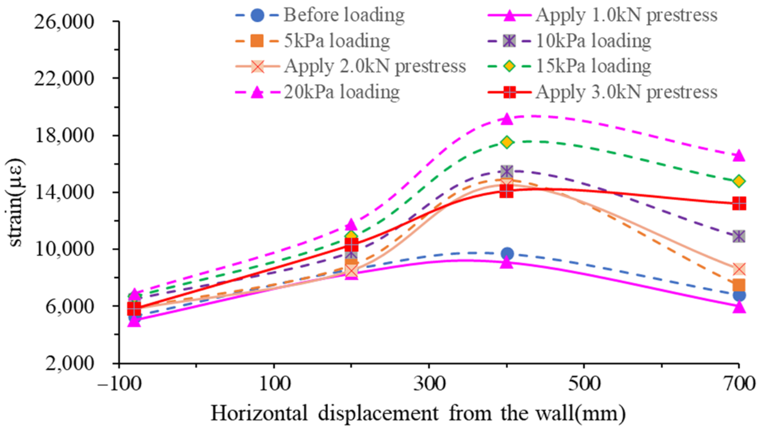

(**g**) Seventh layer of geogrid (Level II wall)

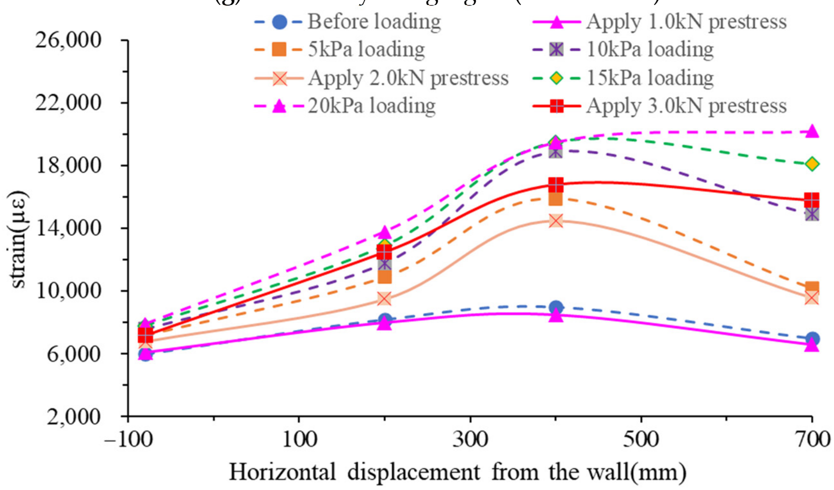

(**h**) Eighth layer of geogrid (Level II wall)

Figure 13. Tensile strain distribution curves of reinforcement along long direction under different load levels.

The distribution shapes of reinforcements vary due to their different locations. In Level I walls, the first and second layers of reinforcements have a relatively close distribution. The strain of these reinforcements shows a slight increase with load changes and is not highly sensitive to them. On the other hand, the third and fourth layers experience a significant strain increase with load changes and are more responsive. The strain increase at the interface between the reinforced soil and the excavation area is minimal. In Level II walls, the fifth to eighth layers of reinforcements exhibit an evenly distributed, peak-shaped distribution. Particularly, there is a notable strain increase at the interface between the eighth layer of reinforced soil and the original slope area, especially after the second loading. This rapid strain increase suggests potential damage at the interface between the reinforced soil and the excavation area.

The results presented in Figure 13 demonstrate that the prestressed anchor rods exert a pulling effect, reducing the horizontal earth pressure on the adjacent layer of geogrids. This reduction leads to a decrease in geogrid strain, ultimately enhancing the load bearing capacity of the geogrid material. The prestressed anchor rods effectively restrain the fill soil under upper loads, facilitating stress transfer within the combined system (Figure 14). This stress transfer mechanism establishes a beneficial synergistic relationship between the reinforced soil, geogrid, and frame beam anchors [25].

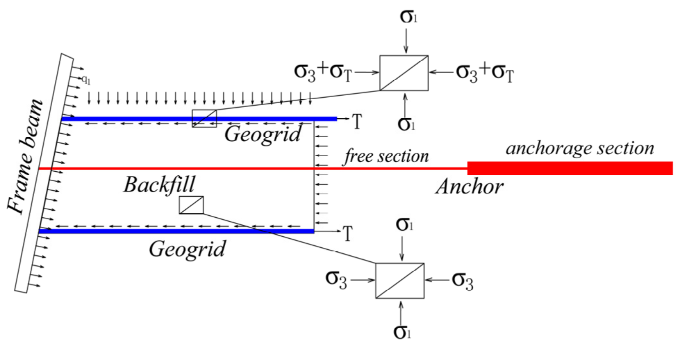

Figure 14. Sketch of interaction between reinforced soil and frame anchor.

3.3. Wall Back Soil Pressure

The distribution curve in Figure 15 illustrates the earth pressure behind the model frame beam. Prior to loading, the earth pressure at the bottom is greater than that at the top. Upon loading, the earth pressure distribution forms a shape resembling a parenthesis, ')', with higher pressure in the middle and lower pressure at the top. This distribution curve closely aligns with the wall displacement and deformation, indicating a relationship between earth pressure distribution and wall deformation.

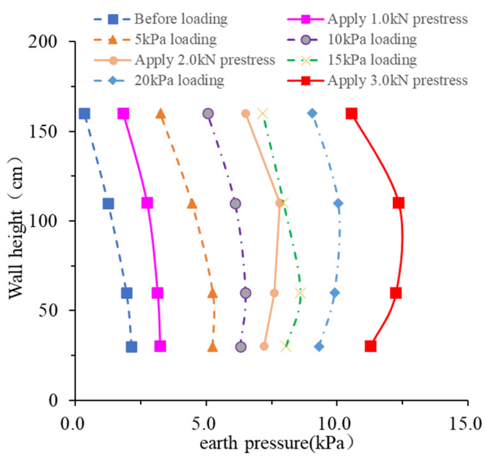

Figure 15. Distribution curves of earth pressure behind model frame beam under different load levels.

Figure 16 illustrates the distribution curve of earth pressure behind reinforced soil. Prior to loading, the earth pressure distribution along the wall height following reinforced soil exhibits a linear trend. With increasing load, there is a slight increase in soil pressure in the upper part, while a significant increase is observed in the lower part. This phenomenon occurs due to the load causing potential separation between the upper and middle sections of the reinforced soil and the excavation area, leading to stress release and reduced soil pressure. Both Figures 15 and 16 demonstrate that the introduction of anchor prestress enhances the earth pressure behind the model frame beam and the reinforced soil. Consequently, the anchor prestress can alter the earth pressure distribution pattern within the system, facilitating a more balanced load distribution. Through stress transmission and transfer, the integrated system can effectively manage the interaction between the reinforced soil and the frame beam anchor, fostering a synergistic relationship.

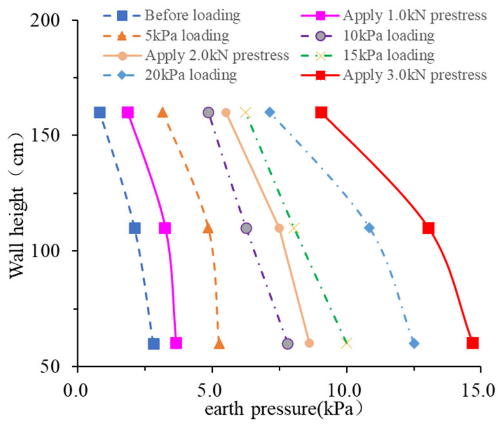

Figure 16. Distribution curves of earth pressure behind reinforced soil under different load levels.

3.4. Anchor Strain

Figure 17 illustrates the strain distribution curve of the anchor along its length. An examination of the anchor curves at different layers reveals that the anchor strain increases proportionally with the load. The strain is highest in the free section, with nearly equal values across this section; the strain in the free section increases significantly with higher loads. Furthermore, the strain in the anchorage section also increases with the load, although the increase is less pronounced. The strain in the anchor for each layer increases accordingly, but to a lesser extent. Notably, the strain in the anchor rod decreases rapidly from the anchoring front end to the anchoring tail end, aligning closely with previous research findings [28,29]. The primary reason for this phenomenon is that as the applied load increases, the tensile force at the end of the anchor rod also increases. The axial force in the free section of the rod is nearly equivalent to the tensile force at the end of the rod, whereas the axial force in the anchored section of the rod decreases non-linearly due to the friction between the anchor material and the soil. Additionally, the strain in the upper part of the retaining wall is generally higher than in the lower part, and the distribution area closely follows the regular distribution area of earth pressure. Experimental results demonstrate that the effect of anchor prestress is characterized by stress transfer, leading to the formation of a synergistic system within the combined structure.

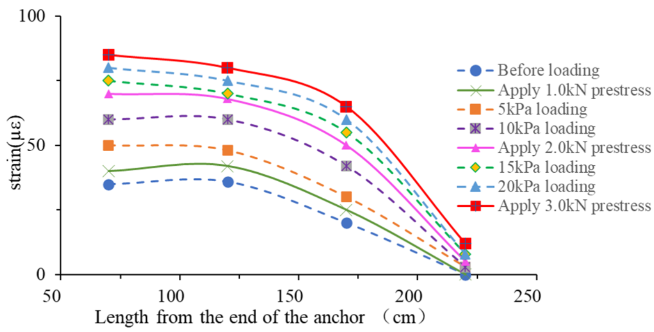

(**a**) M1 anchor rod (Level I wall)

Figure 17. *Cont.*

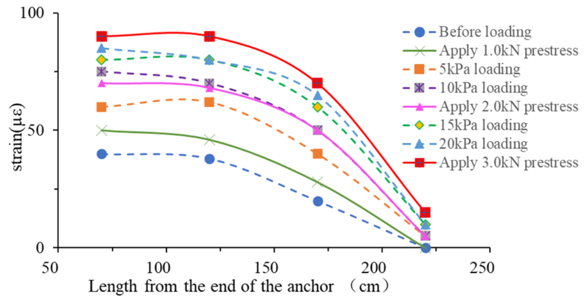

(**b**) M2 anchor (Level I wall)

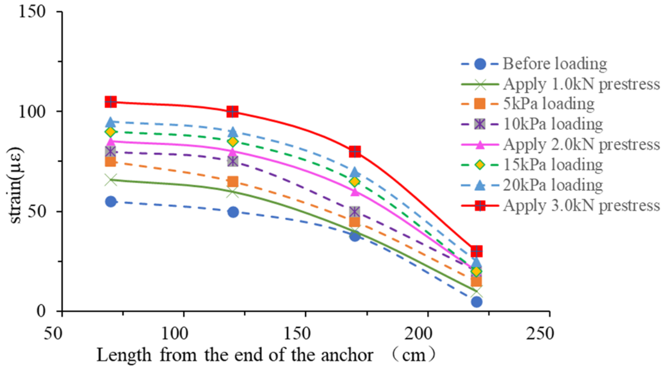

(**c**) M3 anchor (Level I wall)

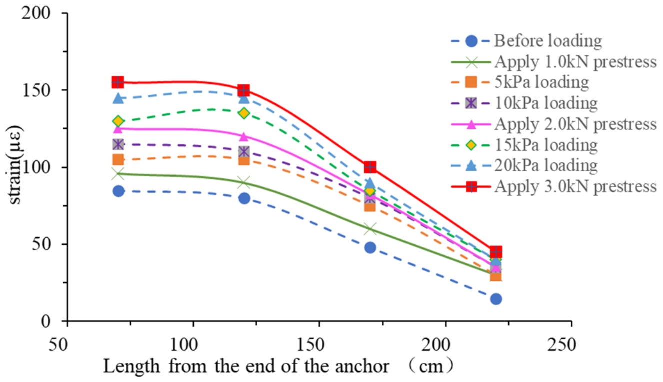

(**d**) M4 anchor (Level II wall)

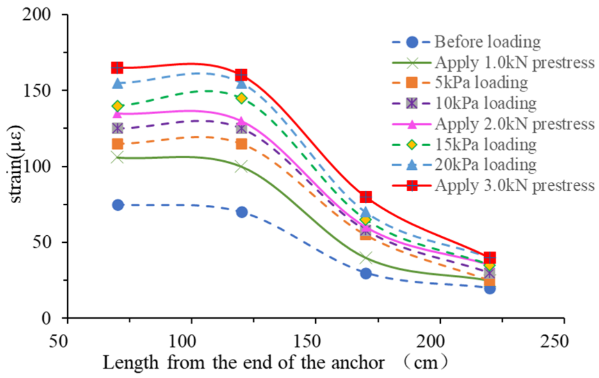

(**e**) M5 anchor (Level II wall)

Figure 17. *Cont*.

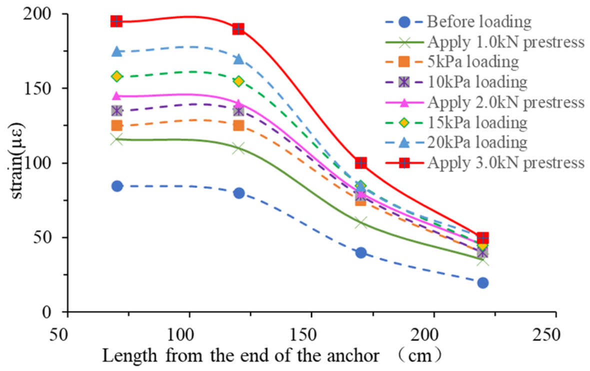

(**f**) M6 anchor (Level II wall)

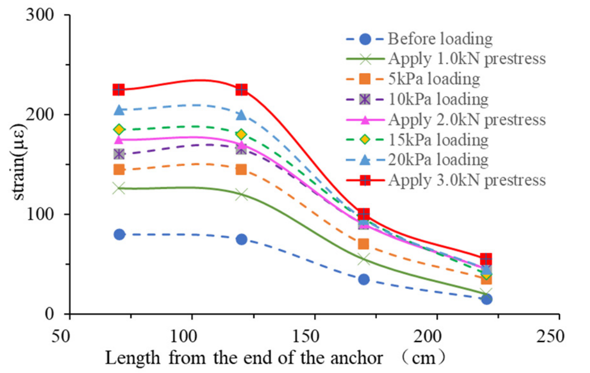

(**g**) M7 anchor (Level II wall)

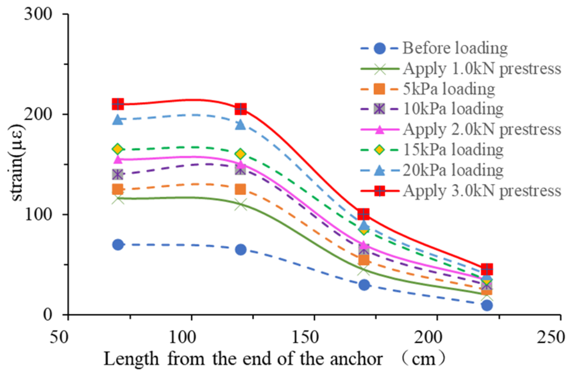

(**h**) M8 anchor (Level II wall)

Figure 17. Tensile strain distribution curves of anchor.

4. Conclusions

This study investigated the mechanical properties of a reinforced soil–frame beam anchor combination system through indoor physical model tests. The study analyzed the patterns of horizontal displacement of the frame beam wall surface, grid strain, wall back soil pressure, and anchor strain. The following conclusions were drawn:

(1) The deformation curves of Level I and Level II walls exhibit a distinct ')' shape, with the highest displacement occurring around one-third of H (where H represents the wall height) from the top of each wall level. Upon the introduction of anchor prestress, the horizontal displacement reaches 65% of the initial displacement value. Experimental results demonstrate that the combined system can yield improved deformation control effects.

(2) As the load increases, the strains in each layer also increase. However, the maximum strain value of the bars is significantly smaller than the designed strain value. Reinforcements play a crucial role in dispersing the additional stress caused by over-

loading on the top of the wall, leading to a more even distribution of earth pressure across each layer and enhancing the wall's stability.

(3) The active constraint effect of prestressed anchor rods effectively shares the additional load, and the application of prestressed anchor rods further reduces the strain of each layer of reinforcements, thereby enhancing the load bearing capacity. This combined system not only increases the external confining pressure of the reinforcement and soil through stress transfer but also establishes a synergistic relationship between the reinforced soil and the frame beam anchors.

(4) The application of anchor prestress enhances the earth pressure behind the model frame beam and the reinforced soil, resulting in a more uniform distribution of earth pressure. Anchor prestress can alter the distribution pattern of earth pressure in the system, facilitating a balanced distribution of loads. Through stress transmission and transfer, the combined system can optimize the interaction between reinforced soil and frame beam anchors, ultimately enhancing overall performance.

Author Contributions: Conceptualization, J.H. and L.Y.; methodology, J.H.; validation, J.H. and L.Y.; data curation, J.H.; writing—original draft preparation, J.H.; writing—review and editing, L.Y.; visualization, J.H. and L.Y. All authors have read and agreed to the published version of the manuscript.

Funding: This work was supported by the Doctoral Startup Fund of Liaoning University of Technology (Grant No. XB2023034).

Data Availability Statement: The datasets are present in the work.

Conflicts of Interest: Author Jiangfei He was employed by the company Shaanxi Institute of Engineering Prospecting. The remaining author declares that the research was conducted in the absence of any commercial or financial relationships that could be construed as a potential conflict of interest.

References

1. Morrison, K.; Harrison, F.; Collin, J.; Dodds, A.; Arndt, B.P. *Shored Mechanically Stabilized Earth (SMSE) Wall Systems Design Guidelines: FHWA-CFL/TD-06-001*; Federal Highway Administration Central Federal Lands Highway Division: Lakewood, CO, USA, 2006.
2. Yang, K.H.; Zornberg, J.G.; Hung, W.Y.; Lawson, C.R. Location of failure plane and design considerations for narrow geosynthetic reinforced soil wall systems. *J. Geotech. Eng.* **2011**, *6*, 27–40.
3. Yang, K.H.; Liu, C.N. Finite element analysis of earth pressures for narrow retaining wall. *J. Geoengin.* **2007**, *2*, 43–52.
4. Yang, K.H.; Kniss, K.K.; Zornberg, J.G.; Wright, S.G. Finite element analyses for centrifuge modeling of narrow MSE walls. In Proceedings of the First Pan American Geosynthetics Conference, Cancun, Mexico, 2–5 March 2008; pp. 1246–1255.
5. Lee, Y.B.; Ko, H.Y.; Mccartney, J. Deformation response of shored MSE walls under surcharge loading in the centrifuge. *Geosynth. Int.* **2010**, *17*, 389–402. [CrossRef]
6. Xu, C.; Luo, Y.; Jia, B.; Chen, H.-S. Effects of connection forms on shored mechanically stabilized earth walls by centrifugal model tests. *Chin. J. Geotech. Eng.* **2016**, *38*, 180–186.
7. Luo, Y.; Xu, C.; Chen, H. Centrifuge Modeling Tests on Behavior of Tiered Shored Mechanically Stabilized Earth Walls. *J. Southwest Jiaotong Univ.* **2016**, *51*, 1163–1169.
8. Xu, C.; Liang, C.; Luo, Y. Stability and failure modes of geosynthetic reinforced soil wall with limited retained backfill. *Hydrogeol. Eng. Geol.* **2017**, *44*, 104–109.
9. Zhou, Y.; Wang, X.; Zhu, Y.; Li, J.; Jiang, X. Contrastive analysis of monitoring and numerical simulation of high slope with interbed of mudstone and sandstone. *J. Lanzhou Univ. Technol.* **2018**, *44*, 109–115.
10. Zhou, Y.; Zhu, Y. Research on anti-pulling force of anchor of flexible supporting system with prestressed anchors. *Rock Soil Mech.* **2012**, *33*, 415–421.
11. Zhou, Y.; Wang, X.; Zhu, Y.; Li, J.; Jiang, X. Monitoring and numerical simulation of an interbedding high slope composed of soft and hard strong-weathered rock. *Rock Soil Mech.* **2018**, *39*, 2250–2258.
12. Fu, X.; Ji, W.; Zhang, J.; Cao, L.; Fan, G. Seismic response for plane sliding of slope reinforced by anchor-chain-framed ground beams through shaking table test. *Rock Soil Mech.* **2018**, *39*, 1709–1719.
13. Dong, J.; Zhu, Y.; Ma, W. Study on dynamic calculstion method for frame supporting structure with prestress anchors. *Eng. Mech.* **2013**, *30*, 250–258.
14. He, S.; Zhang, X.; Ouyang, C. Research of rock high cut slope reinforced by pre-stressed anchorage. *China Civ. Eng. J.* **2011**, *44*, 102–107.

15. Luo, J.; Zhang, D.; Fang, Q.; Li, A.; Liu, D.; Yu, L.; Hong, X. Combined Support Mechanism of Pretensioned Rock Bolt and Anchor Cable for Super-Large-Span Tunnel. *China Railw. Sci.* **2020**, *41*, 71–82.
16. Long, J.; Jiang, B.; Liu, G.; Zhu, Z. Study on the mechanism and application of synergistic anchoring systems in roadway surrounding rocks. *J. China Coal Soc.* **2012**, *37*, 374–378.
17. Du, Y.; Liu, H.; Zhou, F. Mechanical properties of hybrid reinforced soil retaining wall. *J. Cent. South Univ. (Sci. Technol.)* **2018**, *49*, 940–948.
18. Zhang, Z.; Liu, H.; Chen, Y. Development of road micropile-MSE wall system in mountainous areas. *J. Cent. South Univ. (Sci. Technol.)* **2017**, *48*, 1849–1857.
19. Zhang, Z.; Chen, Y.; Liu, H.; Liu, L.; Ye, L. Multivariate analysis of stress and deformation behavior of micropile-MSE wall. *Rock Soil Mech.* **2017**, *38*, 1911–1919.
20. Li, H.; Luo, Q.; Zhang, L.; Jiang, L.; Zhang, J. Centrifugal model tests on shoulder balance weight retaining wall with reinforced earth. *Chin. J. Geotech. Eng.* **2014**, *36*, 458–465.
21. Zhou, J.; Li, C.; Huang, J.; Zhang, J. The deformation law and stress mechanism of wrapped-reinforced and counterfort combined retaining wall. *J. Tongji Univ. (Nat. Sci.)* **2015**, *43*, 529–535.
22. Cao, W.; Zheng, J.; Xue, P. Development of combined retaining structure composed of anti-slide pile and reinforced earth retaining wall. *J. Cent. South Univ. (Sci. Technol.)* **2019**, *50*, 118–129.
23. Wu, H.; Pai, L.; Lai, T.W.; Zhang, J.; Zhang, Y.; Li, Y. Study on cooperative performance of pile-anchor-reinforced soil combined retaining structure of high fill slopes in mountainous airports. *Chin. J. Rock Mech. Eng.* **2019**, *38*, 1–14.
24. He, J.; Yao, L.; Ma, C.; Zhu, Y.; Wu, Z.; Lai, R. Anti-slide Analysis on Composite System of Multi-stage reinforced Soil with Limited backfill and Frame Foundation Beam with Anchor Cable on high-steep loess slope. *Sci. Technol. Eng.* **2019**, *19*, 235–242.
25. He, J.; Yao, L. Model Test Study on Synergistic action of Composite System of Reinforced Soil with Limited Backfill and Frame Foundation Beam with Anchor Cable. *Sci. Technol. Eng.* **2020**, *20*, 14185–14192.
26. Yuan, W. *The Similarity Theory and the Statics Model Test*; Southwest Jiaotong University Press: Chengdu, China, 1998.
27. Xu, T. *The Similarity Theory and the Model Test*; China Agricultural Mechanical Press: Beijing, China, 1982.
28. Jing, F.; Cheng, C.; Yu, M.; Chen, H.; Liu, Y. Load distribution and the Law of Its Variation in the Inner Segment of Prestressed Anchor Cable. *J. Yangtze River Sci. Res. Inst.* **2011**, *28*, 50–54.
29. Li, Y.; Wang, M.; Zhang, D.; Zhang, S. Study on influential factors and model for variation of anchor cable prestress. *Chin. J. Rock Mech. Eng.* **2008**, *27* (Suppl. S1), 3140–3146.